Climate Dynamics (2002) 19: 383–395
DOI 10.1007/s00382-002-0245-9

I.-S. Kang · K. Jin · B. Wang · K.-M. Lau · J. Shukla
V. Krishnamurthy · S.D. Schubert · D.E. Wailser
W.F. Stern · A. Kitoh · G.A. Meehl · M. Kanamitsu
V.Y. Galin · V. Satyan · C.-K. Park · Y. Liu

Intercomparison of the climatological variations of Asian summer monsoon precipitation simulated by 10 GCMs

Received: 17 April 2001 / Accepted: 29 October 2002 / Published online: 4 June 2002

Abstract We assesses the overall performance of state-of-the-art atmospheric GCMs in simulating the climatological variations of summer monsoon rainfall over the Asian-Western Pacific region and the systematic errors that are common to a group of GCMs. The GCM data utilized are obtained from 10 GCM groups participated in the CLIVAR/Monsoon GCM Intercomparison Project. The model composite shows that the overall spatial pattern of summer monsoon rainfall is similar to the observed, although the western Pacific rainfall is relatively weak. For the simulated precipitation over the western Pacific, the models can be classified into two categories. The first category of models simulates the precipitation more confined to the equatorial region and weaker precipitation in the subtropical western Pacific compared to the observed. The second category of models simulates large precipitation in the subtropical western Pacific but the region is shifted to the north by 5–10°. None of the models realistically reproduce the observed Mei-yu rain band in the region from the East China Sea to the mid Pacific. Most of the models produce a rain band along the continental side of East Asia. The climatological variations of simulated summer rainfall are examined in terms of their amplitude and their principal EOF modes. All models simulate larger amplitudes of the climatological seasonal variation of Indian summer monsoon than the observed, though most models simulate smaller amplitudes in the western Pacific. The ten model composite produces four leading EOF modes over the Asian-western Pacific region, which are remarkably similar to the observed counterparts. The first and second eigenmodes, respectively, represent the smoothed seasonal march of broad-scale monsoon and the onsets of the Indian and East Asian

I.-S. Kang (✉) · K. Jin
School of Earth and Environmental Sciences,
Seoul National University, Seoul, 151-742, Korea
E-mail: kang@climate.snu.ac.kr

B. Wang
International Pacific Research Center,
University of Hawaii, Hawaii, USA

K.-M. Lau
Climate and Radiation Branch,
NASA/Goddard Space Flight Center, Greenbelt, MD, USA

J. Shukla · V. Krishnamurthy
Center for Ocean–Land–Atmosphere Studies,
Institute of Global Environment and Society,
Inc., Calverton, MD, USA

S.D. Schubert
Data Assimilation Office, NASA/GSFC,
Greenbelt, MD, USA

D.E. Wailser
Institute for Terrestrial and Planetary Atmospheres,
State University of New York, Stony Brook, NY, USA

W.F. Stern
Geophysical Fluid Dynamics Laboratory/NOAA,
Princeton University, Princeton, NJ, USA

A. Kitoh
Meteorological Research Institute,
Tsukuba, Ibaraki, Japan

G.A. Meehl
National Center for Atmospheric Research,
Boulder, CO, USA

M. Kanamitsu
National Centers for Environmental Prediction,
Camp Springs, MD, USA

V.Y. Galin
Institute of Numerical Mathematics
of Russian Academy of Sciences,
Moscow, Russia

V. Satyan
Indian Institute of Tropical Meteorology,
Pune, India

C.-K. Park
Climate Prediction Division,
Korea Meteorological Administration,
Seoul, Korea

Y. Liu
Institute of Atmospheric Physics, Beijing,
People's Republic of China

summer monsoon. The third and fourth modes relate to the climatological intraseasonal oscillation (CISO). In contrast to the model composite, several models fail to reproduce the first principal mode, and most models do not reproduce the observed modes higher than the second. The CISO of precipitation is also examined over the Indian monsoon and the East Asia-western Pacific monsoon regions separately.

1 Introduction

The Asian monsoon, characterized by sudden wind reversal and onset of heavy precipitation during boreal summer over South and East Asia, provides a major portion of water resources over these most densely populated regions in the world (Ho and Kang 1988; Lau and Li 1984; Lau et al. 1988). The prediction of summer rainfall is thus very important in the monsoon countries. General circulation models (GCMs) have been developed and used for monsoon diagnostic and prediction studies (Shukla and Fennessy 1994; Ju and Slingo 1995: Liang et al. 1995; Zhang et al. 1997; Goswami 1998; Webster et al. 1998; Sperber et al. 2000; Ramesh et al. 2000). Studies have shown that GCM results may be sensitive to physical parametrization (Zachary and Randall 1999) and to model resolution (Sperber et al. 1994; Lal et al. 1997; Martin 1999). For GCMs to be useful for monsoon studies, it is essential that main features of the summer monsoon should be simulated with reasonable accuracy. We assess the overall performance of recent GCMs in simulating the summer monsoon rainfall, particularly focusing on its seasonal evolution, and describe the differences among models by intercomparing their simulations.

Atmospheric Model Intercomparison Project (AMIP) has provided a comprehensive evaluation of the performance of atmospheric GCMs and has proven to be a useful benchmark of model sensitivity and predictability experiments to SST forcing (Slingo et al. 1996; Boyle 1998; Gates et al. 1999). A number of AMIP monsoon intercomparison studies have been conducted previously. Sperber and Palmer (1996) found that AMIP GCMs which have a better rainfall climatology generally simulate better the interannual variability of rainfall. Gadgil and Sajani (1998), and Soman and Slingo (1997) showed that realistic simulation of variability in the western Pacific may be a key to simulate strong or weak monsoons associated with ENSO. However, the performance of GCMs with regard to the impacts on the monsoon by the exceptional ENSO of 1997–98 has not been evaluated. Recently, the CLIVAR/Asian Australian Monsoon Panel has initiated a monsoon GCM intercomparison project, focusing on the ENSO/Monsoon anomalies associated with the 1997–1998 El Niño (Kang et al. 2002). To obtain the climatological annual cycle and the 1997–1998 anomalies, the monsoon intercomparison project has requested each participating group to carry out an AMIP type simulation for the 20-year period from 1979–1998. The intercomparison results for the 1997–1998 ENSO anomalies are documented in Kang et al. (2002). The present study, on the other hand, is aimed at documenting the climatological variations of summer rainfall over the Asian monsoon region obtained from the 20-year simulations.

The climatological seasonal variations are the most distinctive phenomena among many complex time scales of variations in the Asian monsoon region (Lau et al. 1988). This climatological cycle is characterized not by a simple smooth variation but by rather complicated variations with diverse regional characteristics. In particular, the climatological onset dates of regional rainy season are different for different regions of the Asian monsoon and appear to propagate northward (Tao and Chen 1987; Tanaka 1992; Lau and Yang 1996). It is also well known that the monsoon rain bands associated with the regional features undergo abrupt changes and appear at different phases of the monsoon cycle (Tao and Ding 1981; Lau and Li 1984). Kang et al. (1999) demonstrate that the regional rain bands are linked to large-scale monsoon rainfall patterns by showing the principal modes of climatological variations of the Asian summer monsoon. Recently, several investigators have shown that the climatological variations of the Asian summer monsoon include distinctive intraseasonal components on top of the smoother seasonal cycle (Krishnamurti 1985; Wang and Xu 1997; Kang et al. 1999). The phase-locked intraseasonal variations appear to control the climatological onset dates of the rainy season over much of the Asian monsoon region (Kang et al. 1989; Nakazawa 1992; Wang and Xu 1997; Kang et al. 1999). All of these previous studies have demonstrated that the climatological variations of Asian summer monsoon rainfall exhibit diverse temporal and spatial characteristics, which should be represented reasonably well by the models if dynamical forecasts of the Asian monsoon are to be skillful.

In the present study, we examine the ability of current GCMs in simulating the complex climatological variations of Asian monsoon rainfall and the regional rain bands, particularly over the Indian and western Pacific monsoon regions. In the present intercomparison, we do not focus on the simulations of specific events or processes of the summer monsoon, nor do we emphasize the results of individual models here. Rather, we focus on the performance of the models as a whole and seek to summarize the systematic errors that are common to a group of atmospheric GCMs in simulating the climatological variation of the Asian summer monsoon.

Section 2 describes the model data obtained from the CLIVAR/GCM Monsoon Intercomparison Project and the observed data utilized in the present study. Section 3 examines the climatological summer mean precipitation simulated by various GCMs. Section 4 examines the climatological rainfall variations during boreal summer from May to September and assesses the models' ability to reproduce the observed leading empirical orthogonal

function (EOF) modes of the climatological variations over the Asia-Pacific sector. Section 5 examines the climatological intraseasonal variations simulated by the models, particularly along the longitudes of 90°E (Indian region) and 130°E (East Asia and the western Pacific). Summary and concluding remarks are given in Sect. 6.

2 Experimental set up and data

As part of the CLIVAR/GCM Monsoon Intercomparison, all participating GCM groups have carried out a 20-year integration with the observed SST from 1 January 1979 to 31 December 1998, to derive the model's climatological annual cycle. The SST data used are the observed pentad means from the Global Sea Ice and Sea Surface Temperature (GISST) data set (Parker et al. 1995) created by the Hadley Centre for Climate Prediction for the period up to January 1979–October 1981 and the Optimum Interpolation Sea Surface Temperature (OISST) analyses data set (Reynolds and Smith 1994) created by the Climate Prediction Center of the National Centers for Environmental Prediction (NCEP) for the period November 1981–December 1998. Because of the unavailability of the data for recent years, the sea ice is prescribed by the climatological monthly mean data utilized by AMIP. Thus the experimental set up of the present intercomparison project is the same as that of the AMIP. Ten institutes from six countries, including COLA, DNM, GEOS, GFDL, IAP, IITM, MRI, NCAR, SNU, and SUNY/GLA have participated in the intercomparison project, which has provided the data for the present study. The descriptions of the participating models are given in Table 1. The details of the intercomparison project and the physical parametrizations adapted in each model can be found in Kang et al. (2002).

The climatological seasonal cycle data is obtained from the average of 20 years of data for each calendar day, and the pentad data utilized in the present study are obtained from the climatological daily data. The variables used are precipitation and 850 hPa stream function. This study focuses on the boreal summer spanning the five months from May to September. Although the spatial resolution of the models varies from rhomboidal truncation at wave number 15 to triangular truncation at wave number 42 (see Table 1), all GCM data were converted to a spatial resolution of 2.5° lat × 2.5° lon. To compare the GCM results with observations, we used the CPC Merged Analysis of precipitation (CMAP; see documentation by Xie and Arkin 1997) and the 850 mb stream function from the National Centers for Environmental Prediction (NCEP) reanalysis database (Kalnay et al. 1996). The CMAP data utilized are the pentad data for the 20 year period from 1979 to 1998. It is noted that the CMAP precipitation is an estimate based on satellite data and in situ observations in the continents (Xie and Arkin 1997). However, there are some differences between the CMAP and another estimate such as the Global Precipitation Climatology Project (GPCP) precipitation, particularly over the ocean regions, because of different algorithms used to retrieve the rainfall from the satellite data. Some of distinctive differences occur in the western Pacific (Gruber et al. 2000). However, most of the conclusions here are not sensitive to the choice of the precipitation data. The observational issue of the 850 mb stream function may be less sensitive to the choice of the NCEP reanalysis, since there should be little difference between the NCEP and European Center for Medium-Range Weather Forecast (ECMWF) reanalyses in the rotational flows.

3 Climatological summer mean precipitation

This section examines how well the models simulate the climatological mean precipitation for the northern summer. Before examining each model result, the all-model composite of climatological summer-mean (June, July and August) precipitation is made by averaging the ten model results, and it is compared with the corresponding observations. The model composite of the summer-mean precipitation shown in Fig. 1a has a spatial pattern similar to that of the CMAP precipitation shown in Fig. 1b, although there are certain differences, especially in the western Pacific. Over the South China Sea and the subtropical western Pacific, where maximum precipitations appear in the observations, the model precipitation is rather weak compared to the observed. The difference is also seen in the location of the large precipitation belt in the subtropical western Pacific, where the belt of the model composite is shifted to the north about 5° compared to the observed. Over the Bay of Bengal and off the west coast of India, on the other hand, the model composite reproduces reasonably well the observed heavy precipitation. But the model precipitation over the regions shows a broader spatial structure. As a result, the observed minimum precipitation off the southeast coast of India

Table 1. Description of the atmospheric GCMs participating in the CLIVAR/Asian-Australian Monsoon GCM intercomparison project

Model	Institution	Resolution	Convection
COLA	Center for Ocean–Land–Atmosphere Studies (USA)	R40, L18	Relaxed Arakawa-Schubert scheme (Moorthi and Suarez 1992)
DNM	Institute of Numerical Mathematics (Russia)	4 × 5°, L21	Convective adjustment scheme (Betts 1986)
GEOS	NASA/GSFC (USA)	2 × 2.5°, L43	Relaxed Arakawa-Schubert scheme
GFDL	Geophysical Fluid Dynamics Laboratory (USA)	T42, L18	Relaxed Arakawa-Schubert scheme
IAP	Institute of Atmospheric Physics (China)	R15, L9	Moist convective adjustment scheme (Manabe et al. 1965)
IITM	Indian Institute of Tropical Meteorology (India)	2.5 × 3.75°, L19	Mass flux scheme (Gregory and Rowntree 1990)
MRI	Meteorological Research Institute (Japan)	4 × 5°, L15	Arakawa-Schubert scheme (Arakawa and Schubert 1974)
NCAR	National Center for Atmospheric Research (USA)	T42, L18	Mass flux scheme (Zhang and McFarlane 1995)
SNU	Seoul National University (Korea)	T31, L20	Relaxed Arakawa-Schubert scheme
SUNY	State University of New York (USA)	4 × 5°, L17	Arakawa-Schubert scheme

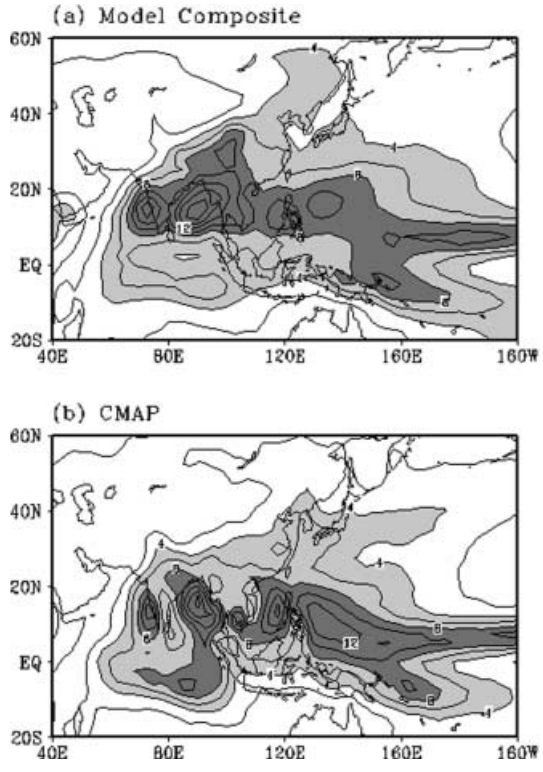

Fig. 1a, b. Distribution of climatological summer-mean precipitation for June, July, and August; **a** and **b** are for the model composite and the observation from CMAP data, respectively. Contour interval is 2 mm day^{-1}. *Light* and *dark shadings* indicate the rainfall rate more than 4 mm day^{-1} and 8 mm day^{-1}, respectively

is not very distinctive in the model composite. Also note that in East Asia the simulated rain band locates along the landward side of the east coast of Asian continent. However, the observed rain band exhibits a zonally elongated structure extending from Eastern China to the mid Pacific. Overall, as indicated, the simulated regional details are somewhat different from the observed counterparts, but the major features of the precipitation distribution are reasonably well captured by the model composite.

The performance of each model in simulating the climatological summer-mean precipitation is examined in Fig. 2. To facilitate the comparisons, the CMAP and model composite shown in Fig. 1 are repeated in Fig. 2a, b, respectively. All models show precipitation maxima in the Indian Ocean and western Pacific monsoon regions. However, regional details differ from one model to another. For example, the precipitation distribution simulated by the COLA model (Fig. 2c) has quite different characteristics from that of the DNM model (Fig. 2d). The precipitation intensity of the COLA model is much stronger than that of the DNM in the Indian region and the western Pacific. The observed belt of heavy precipitation located in the subtropical western Pacific is shifted to the equator in the DNM model, whereas it is shifted slightly to the north in the COLA model. Although there are some differences among models, most of the models simulate excessive precipitation in the Indian region. On the other hand, several of the models simulate weak precipitation over the subtropical western Pacific (e.g., IAP and MRI). The models can be classified into two categories according to the western Pacific precipitation. The models of one category simulate the precipitation maximum in the equatorial Pacific but weak precipitation in the subtropical western Pacific, the region of heavy precipitation in the observations. This category includes the models of DNM, IAP, NCAR, and MRI. The models of the other category, including the COLA, GEOS, IITM, and SNU models, simulate excessive precipitation in the subtropical western Pacific but the maximum precipitation region is shifted to the north by 5–10° compared to the observations. The GFDL and SUNY/GLA models simulate the western Pacific precipitation more or less in the right location. However, those models produce heavy precipitation in the Indochina peninsula where relatively light precipitation is observed. Note that none of the models reproduces the observed precipitation band in the region from the East China Sea to the mid-Pacific. Most of the models simulate a considerable precipitation band on the continental side along East Asia with a dry area extending from the Sea of Okhotsk to the Korean peninsula. This discrepancy has been noted in the AMIP-I intercomparison of the Asian monsoon (Lau et al. 1996).

The two categories classified according to the simulation of western Pacific precipitation are more clearly shown in Fig. 3. The figure shows the composites of the four models for each category. In the figure, the 850 hPa stream function is plotted on top of the precipitation (shaded). The model composite of COLA, GEOS, IITM, and SNU shown in Fig. 3b (first category) produce a stronger than observed monsoon circulation around the Asian continent (Fig. 3a). Accordingly, the monsoon precipitation over the Indian region and the western Pacific is larger than the observations. In particular, the strong monsoon westerlies penetrate all the way to the western Pacific to about 150°E, resulting in heavy precipitation in the subtropical western Pacific. However, the center of the precipitation is shifted to the north in the western Pacific by about 5° compared to the observations. Also note that the model composite in Fig. 3b shows a ridge line penetrating to Japan and Korea from the center of the Pacific high. This causes the models to be dry over the region of the observed rain band near Japan and pushes the rain band to the continental side. For the models of DNM, IAP, MRI, and NCAR (second category), on the other hand, the simulated Asian monsoon circulation is rather weak, resulting in light precipitation in both in India and the western Pacific (Fig. 3c). Clearly, the weak precipitation in the subtropical western Pacific is related to the abnormal strength of the Pacific high extending to the South China Sea, which prevents the monsoon westerlies reaching the western Pacific. For those models, the

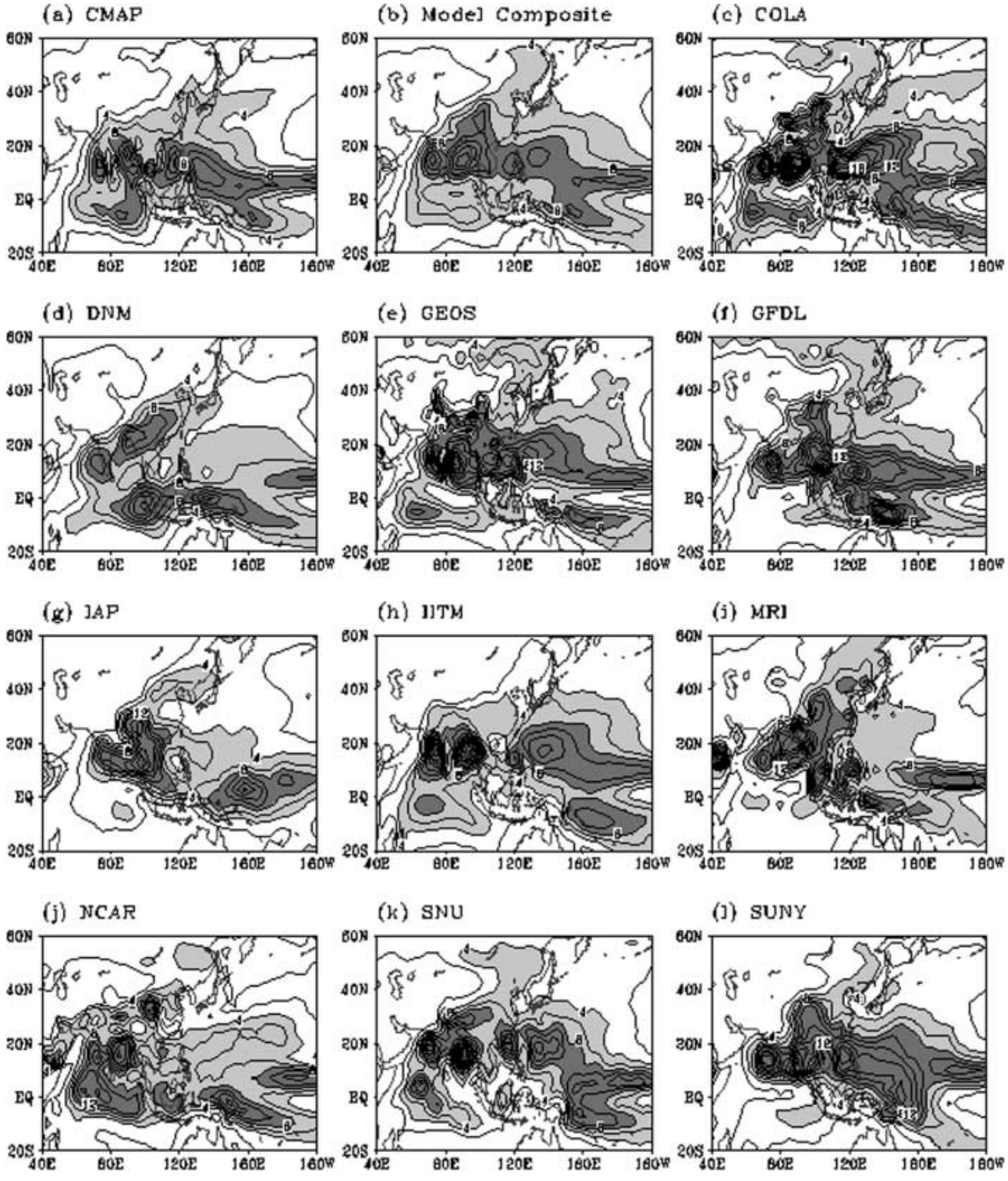

Fig. 2a–l. As in Fig. 1a but for various GCMs

subtropical western Pacific is occupied by the ridge, which pushes the rain band to the equatorial region. The comparison of the two categories of model simulations suggests that the strength of Asian monsoon circulation relative to the Pacific high strongly affects the monsoon westerlies and precipitation in the subtropical western Pacific. This finding is consistent with previous results which showed that better simulation of the Asian monsoon in AMIP GCMs is dependent upon how well the models simulate the northward migration of the convective zone over the tropical western Pacific (e.g., Gadgil and Sajani 1998; Soman and Slingo 1997).

The different performance of the two model groups should be related to the physical parametrizations, particularly for the convection, adapted in the models. All models of the first category use the Arakawa-Schubert scheme for the convection. The GFDL and SUNY/GLA models also use the Arakawa-Schubert scheme, which appears to simulate the precipitation distribution in the western Pacific more reasonably than other schemes do. On the other hand, the models of the second category use different convection schemes (Table 1). It is pointed out that the MRI model uses the Arakawa-Schubert scheme, although the model belongs to the

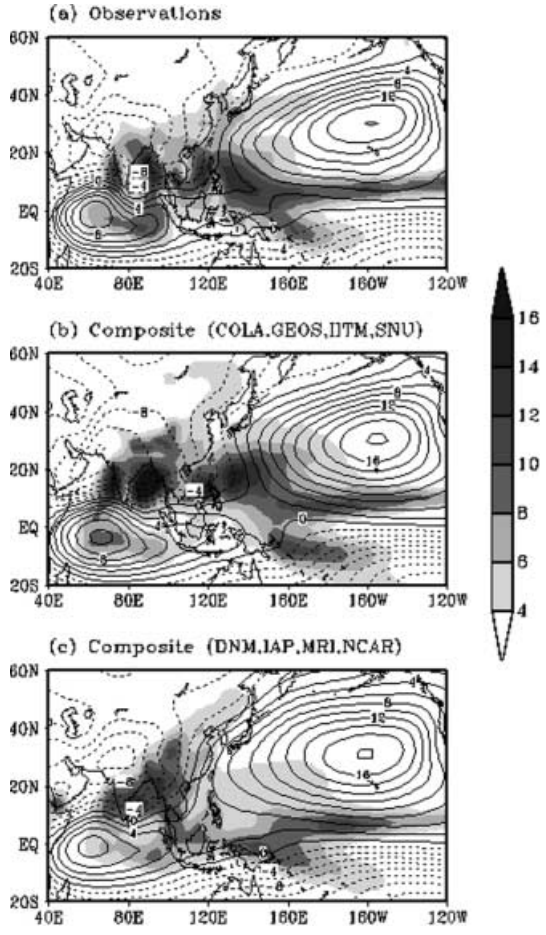

Fig. 3. **a** Climatological summer mean precipitation and NECP 850 hPa streamfunction for the observations. **b** As in **a** except for the four model composites of COLA, GEOS, IITM, and SNU, and **c** for the composites of DNM, IAP, MRI, NCAR. Precipitation is *shaded*. The precipitation scale (mm day^{-1}) is shown in the bar at the *right side* of the figure. Unit of the stream function is 10^6 m^2 s^{-1}

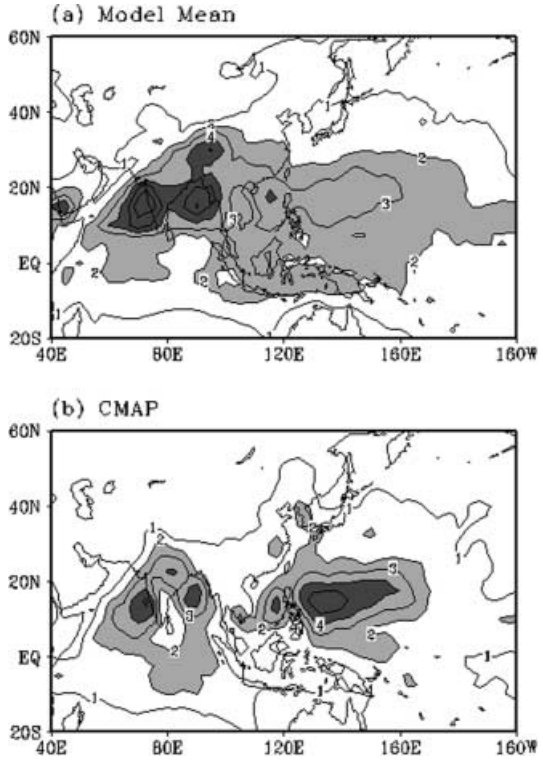

Fig. 4. Standard deviation of climatological variations of pentad-mean precipitation for the five months from May to September; **a** and **b** are for the average of the ten model standard deviations and for the CMAP observations, respectively. Contour interval is 1 mm day^{-1}. *Light* and *dark shadings* indicate the standard deviations larger than 2 mm day^{-1} and 4 mm day^{-1}, respectively

second category. This indicates that physical parametrizations other than the convection scheme also play important roles in the simulation of precipitation over the western Pacific.

4 Climatological variations from May to September

In this section, the climatological variations of precipitation during boreal summer simulated by various GCMs are examined by analyzing the pentad data of the 20 year mean climatological cycle from May to September. In particular, the amplitude of the variation is examined in terms of the standard deviation from the summer mean. Figure 4a shows the average of the 10 standard deviations produced by the GCMs. This is compared to the corresponding standard deviation of CMAP precipitation shown in Fig. 4b. The models generally capture the large climatological variations over the Asian monsoon region. However, the amplitude of the simulated variations in the western Pacific is weaker than that of the observed. On the other hand, the simulated variations over India and the surrounding oceans are stronger than the observed.

We next examine how the variability of each model distributes along the subtropical latitude belt, where both the observed and model climatological cycles show large variations. Figure 5 shows the standard deviation of each model for the latitudinal means between 10 and 20°N. The thick black line indicates the observed CMAP standard deviations along the subtropical belt between 40°E and 160°W. The figure clearly shows that in the Indian region (70–100°E), most of models overestimate the amplitude of the climatological variations. In the western Pacific, on the other hand, most of the models simulate weaker variations. In particular, the model variations of DNM, NCAR, MRI, and GEOS are significantly weaker than those of the observed. As shown in the previous section, these models, except GEOS, simulate weak summer-mean precipitation in the western Pacific. The other groups of models, such as SUNY/GLA, COLA, SNU, and IITM, which simulate relatively large summer-mean precipitation, produce reasonable amplitudes of the climatological variations in the western Pacific. These results indicate that the simulated climatological variability depends on the model ability of simulating the climatological mean, consistent with previous results (Sperber and Palmer 1996).

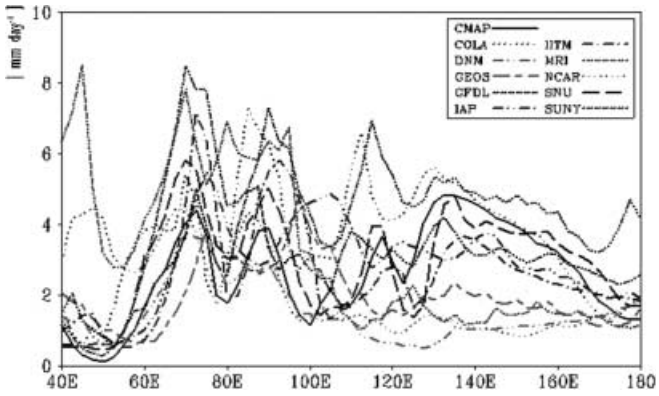

Fig. 5. Longitudinal distribution of the standard deviation of climatological pentad-mean precipitation from May to September, for the latitudinal mean of 10–20°N. The *lines*, illustrated at the *right upper corner* of the figure, indicate the standard deviation of each model

The principal modes of the climatological variations of precipitation over the Asian-Pacific region are examined using the results from the empirical orthogonal function (EOF) analysis of the climatological mean pentad data from May to September. Figure 6 shows the four leading EOF eigenvectors of the model composite (Fig. 6a–d) and the observations (Fig. 6e–h). The model composite reproduces the observed four leading eigenvectors with reasonable accuracy. The first eigenvector shows simultaneous development and decay of the Indian and western Pacific monsoons representing the seasonal march of broad-scale monsoon. Consistent with results in the previous section, the magnitudes of the model eigenvector in the western Pacific are smaller than those of the observed. The time series associated with the eigenvector (Fig. 6i) shows earlier development of the model monsoon. The peak phase of the model composite appears about one month earlier than that of the observed. The second eigenmode represents the onset of the Indian monsoon, with a linkage to the East Asian rainband. Kang et al. (1999) obtained an eigenvector similar to the present second one using the observed high cloud data, and they related the mode to the onset of the Baiu-Meiyu rain band. The time series of the second mode of the model composite is much smoother than the observed, and the onset timing and peak phase are somewhat earlier in the model than those in the observations. The observed third (Fig. 6g) and fourth (Fig. 6h) modes appear in the model as the fourth (Fig. 6c) and third (Fig. 6d) modes, respectively. Although the order of the modes is interchanged, the model composite reproduces the observed third and forth modes reasonably well. As noted in Kang et al. (1999), the observed third mode may be related to the climatological intraseasonal oscillation (CISO) of the Asian summer monsoon. Although the associated time series of the model composite shown in Fig. 6k and l are much smoother than the observed counterparts, the major fluctuations appear to agree well.

We next examine how each model produces the leading eigenmodes. The first eigenvectors simulated by individual models are shown in Fig. 7. For easy comparisons, those of the observed and model composite are included in Fig. 7a, b. Many models reproduce the observed first eigenvector reasonably well. However, several models including COLA, DNM, MRI, and NCAR produced the first eigenvector somewhat different from the observed. The percent variance explained by the first eigenvector ranges from about 40 to 55 % of the total variance of the individual model. The time series associated with the first eigenvector of each model (Fig. 7m) describe the seasonal march of the northern summer, having negative values in May and early June and large positive values in late July and early August. Overall, the results shown in Fig. 7 indicate that many but not all models reproduce the major spatial pattern of the observed seasonal march of the Asian summer monsoon.

The pattern correlations between the eigenvectors of individual models and the observed counterparts are shown in Fig. 8. The correlations for the first eigenvector are shown with a black bar. The pattern correlations of the second, third, and forth eigenvectors are also shown in Fig. 8 with different bars. As in the model composite, the third and fourth modes produced by some of the models are similar, respectively, to the observed fourth and third modes. For those models, the pattern correlations of the third and fourth eigenvectors are computed with the observed fourth and third eigenvectors, respectively. All correlation values of the model composite are quite high. But most of the models have a large correlation only for the first eigenvector but not for the higher modes. One exception, the SNU model, appears to reproduce all of the observed leading eigenmodes reasonably well. The SUNY/GLA model reproduces the first and second modes most realistically. It is also noted that the MRI and NCAR models poorly simulate the first eigenvector but produce the second and third eigenvectors better than those of the other models.

5 Climatological intraseasonal variations

It is well known that the Asian monsoon is dominated by the two components, namely the Indian monsoon and the western Pacific-East Asian monsoon (Lau and Li 1984; Wang et al. 2001). Over these regions, the climatological rainfall variations undergo abrupt changes, which are the characteristic feature of monsoon onset, and have significant intraseasonal components (Wang and Xu 1997). These climatological intraseasonal variations control the climatological onset date of regional rainy seasons over India and East Asia (Nakazawa 1992; Kang et al. 1999). In this section, we show how the intraseasonal components appear in the climatological variations, particularly along the longitude belts covering India (90°E) and East Asia (130°E). Note that the longitudes along 90°E and 130°E cross the centers of large climatological variability, shown in Fig. 4. Figure 9a, b shows the time-latitude

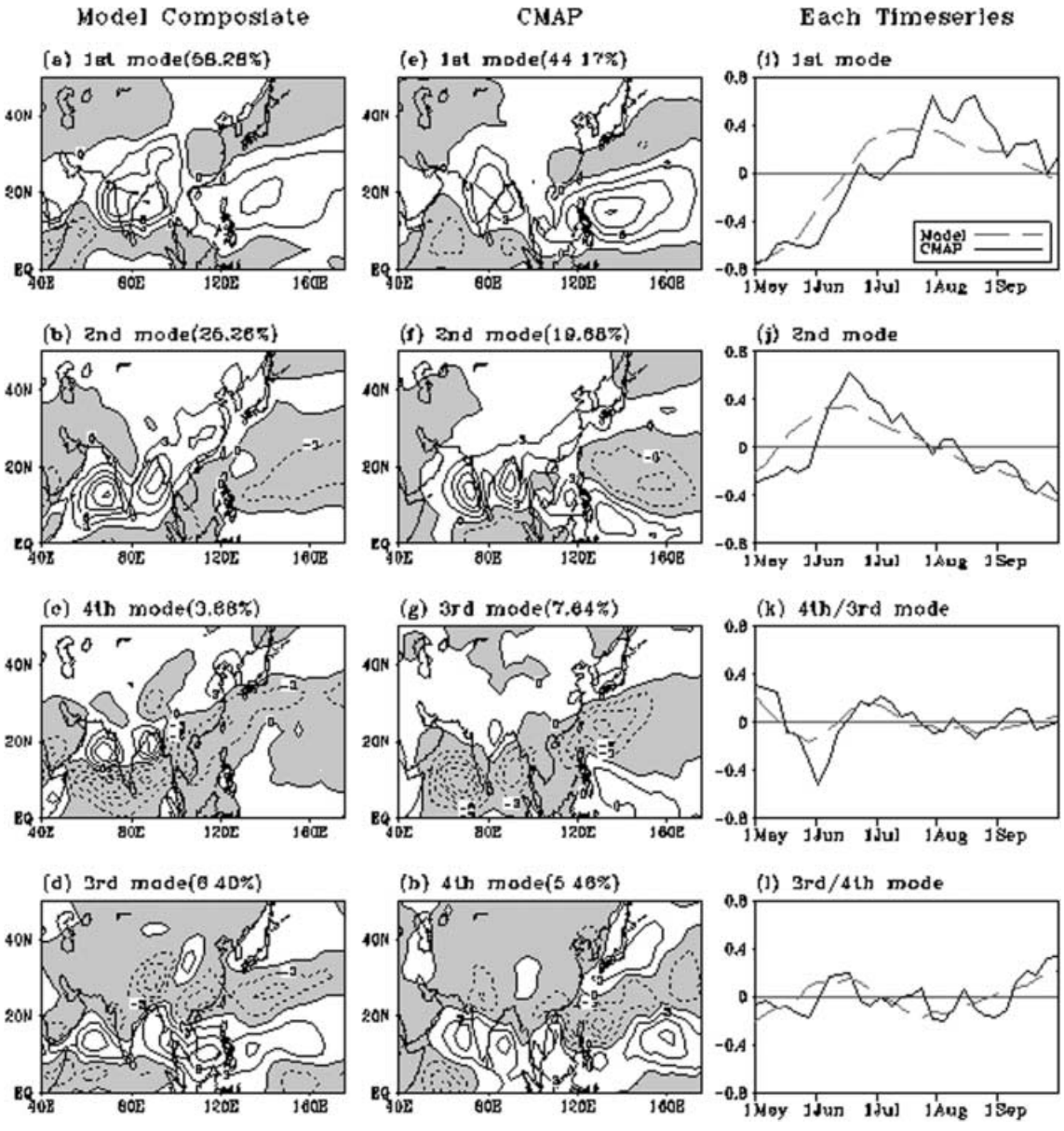

Fig. 6. Four leading EOF eigenvectors and associated time series of the climatological pentad-mean precipitation for May–September; **a**–**d** are for the model composite, and **e**–**h** for the CMAP observations. The associated time series of CMAP and the model composite are shown in **i**–**l** with a *line* and a *dashed line*, respectively. Units are arbitrary

cross sections along 90°E for the model composite and the CMAP observations, respectively. The model composite produces the sudden onset of Indian monsoon in early May, which is similar to the observed. The mature phase of the model lasts until early July and the rainfall rate decays afterward. In the observations, on the other hand, maximum precipitation appears intermittently in June, July and August, indicating the existence of climatological intraseasonal oscillation (CISO). The CISO is more evident near the equator and tropical Southern Hemisphere in the observations, but the CISO is missing in the model composite.

Along 130°E longitude, the model composite (Fig. 9c) is characterized by the maximum precipitation located at the equator during spring until late May, with a sharp transition to the latitude 10–15°N in early June, where it stays until the end of summer. Although this model behavior is also seen in the observations (Fig. 9d), there are certain differences between the two figures. The jump of rain belt in the subtropical western Pacific appearing in early June is less sudden in the observations, where enhanced precipitation appears off the equator during early June and then propagates northward until the end of August. This northward progression does not appear in the model composite. In the observations, The northward propagations of rain band and dry zone are also evident in the extratropics between 15°N and 40°N during the summer. This extratropical character is largely missing in

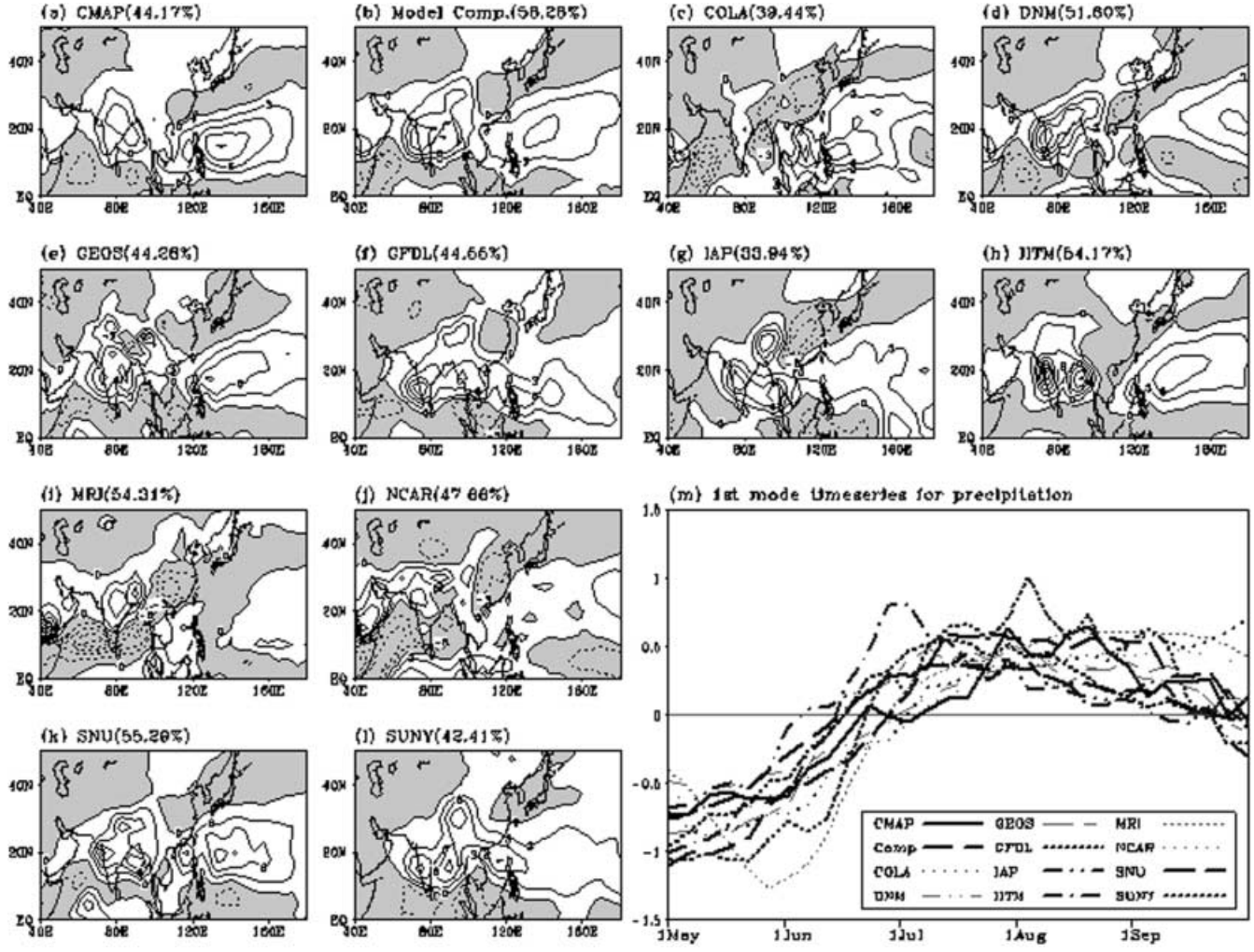

Fig. 7a–m. As in Fig. 6a, except for the first EOF eigenvector of each model. For comparison, the first eigenvectors of CMAP and model composite are shown in **a** and **b**, respectively. The time series of each model are shown in **m**

the model composite. Kang et al. (1999) showed that the northward movement of the extratropical rain band strongly affects the rainy seasons in East Asia. They ascribed this alternative appearance of rain band and dryness to the climatological intraseasonal oscillation with a time scale of about two months. The absence of the extratropical CISO in the model composite can be due to the cancellation of the CISO's of individual models having slightly different phases from each other. To check this possibility, we examine the CISO's of individual models along the 130°E longitude line.

Figure 10 shows the time-latitude cross sections of the CISO component of precipitation along 130°E for the CMAP observations (Fig. 10a), the model composite (Fig. 10b), and individual models (Fig. 10c–l). As in Kang et al. (1999), the CISO component is obtained by removing the smooth seasonal cycle, the sum of first four harmonics of the climatological cycle, from the original climatological cycle. In the CMAP, the large positive anomalies near 20°N appearing in mid-May propagate northward up to 40°N. The dry anomalies following the rain band locate at 20°N in early June and at 40°N in early August. The positive CISO anomalies again follow the negative anomalies between 20 and 40°N. This northward propagating character of the CISO component can be found in the model composite, but it is generally very weak and the phase is shifted so that the model CISO occurs 20–30 days earlier than the observations. Several models such as COLA, GEOS, IITM, and SNU show the northward moving CISO components, which have equivalent amplitudes to those of the CMAP, though the CISO's simulated by several models are very weak. The SUNY model simulates the tropical CISO reasonably well but poorly reproduces the extratropical CISO.

The mean amplitude of the CISOs simulated by the models is obtained by the average of the ten standard deviations (std) of the CISO component computed separately with ten individual models. Figure 11a shows the model averaged standard deviations of the CISO. For comparison, the observed counterpart of the CMAP data is shown in Fig. 11b. The spatial distribution of the

model std over the Asian Pacific region is similar to the observed distribution, although the model std are rather weak in the western Pacific. In particular, the observed large CISO components appearing off the east coast of China are not evident in the models, indicating that the present models simulate the extratropical CISO more weakly than the observed. In the Indian monsoon region, the models reproduce the relatively large amplitudes of the observed CISO. However, over the tropical Indian Ocean region, particularly in the Southern Hemisphere, the model simulated CISOs are much weaker than the observed.

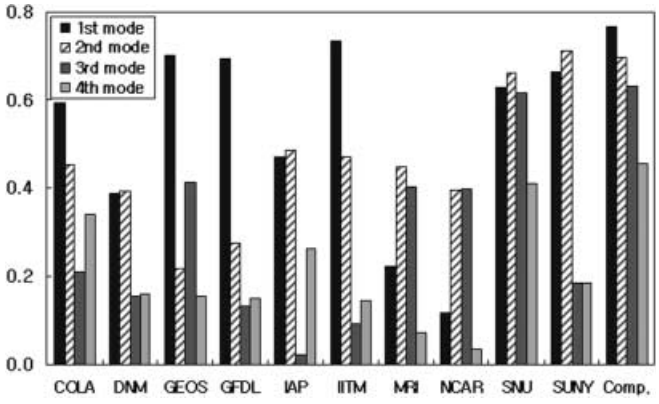

Fig. 8. Pattern correlations between the EOF eigenvectors of CMAP observation and the corresponding eigenvectors of individual model over the domain of 40°E–160°E and Eq. –40°N. The correlation values for the first, second, third, and forth eigenvectors are shown by the bars with different *shadings*. See details in text

6 Summary

In this study, we examined the ability of ten state-of-the-art GCMs to simulate the climatological variations of large-scale monsoon rainfall and the regional rain bands in India and East Asia. All the model composites show the large-scale spatial pattern similar to the corresponding observations and are better than any individual model results. The regional structures of the climatological mean precipitation simulated by individual models differ substantially from the observed. All models produce excessive rainfall in the Indian monsoon region. In the subtropical western Pacific, a group of models including DNM, IAP, NCAR, and MRI fail to reproduce the observed large precipitation. In this group, large precipitation region is confined to the equatorial region of the western Pacific and the Indian monsoon tends to be weaker. A second group of models which include COLA, GEOS, IITM, SNU, simulate more precipitation in the subtropical western Pacific but their heavy precipitation region is somewhat shifted to the north compared to the observed. These models tend to produce a stronger Indian monsoon compared to the previous group. The realistic simulation of the seasonal movement of the western Pacific subtropical high appears to be crucial for an overall simulation of the Asian

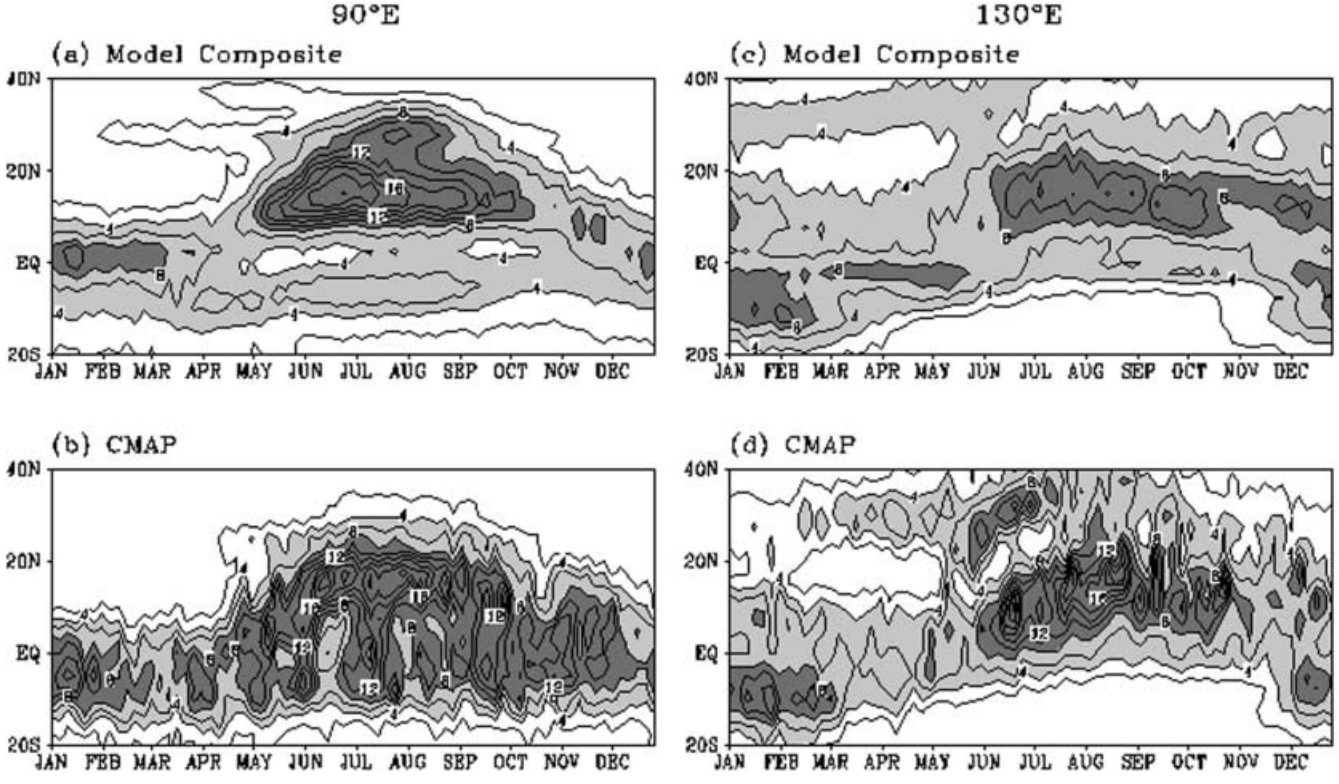

Fig. 9. Time-latitude cross section of climatological pentad-mean precipitation along 90°E and 130°E: **a** and **b** are, respectively, for the model composite and the CMAP observations along the latitude of 90°E; **c** and **d** are as in **a** and **b** but for 130°E

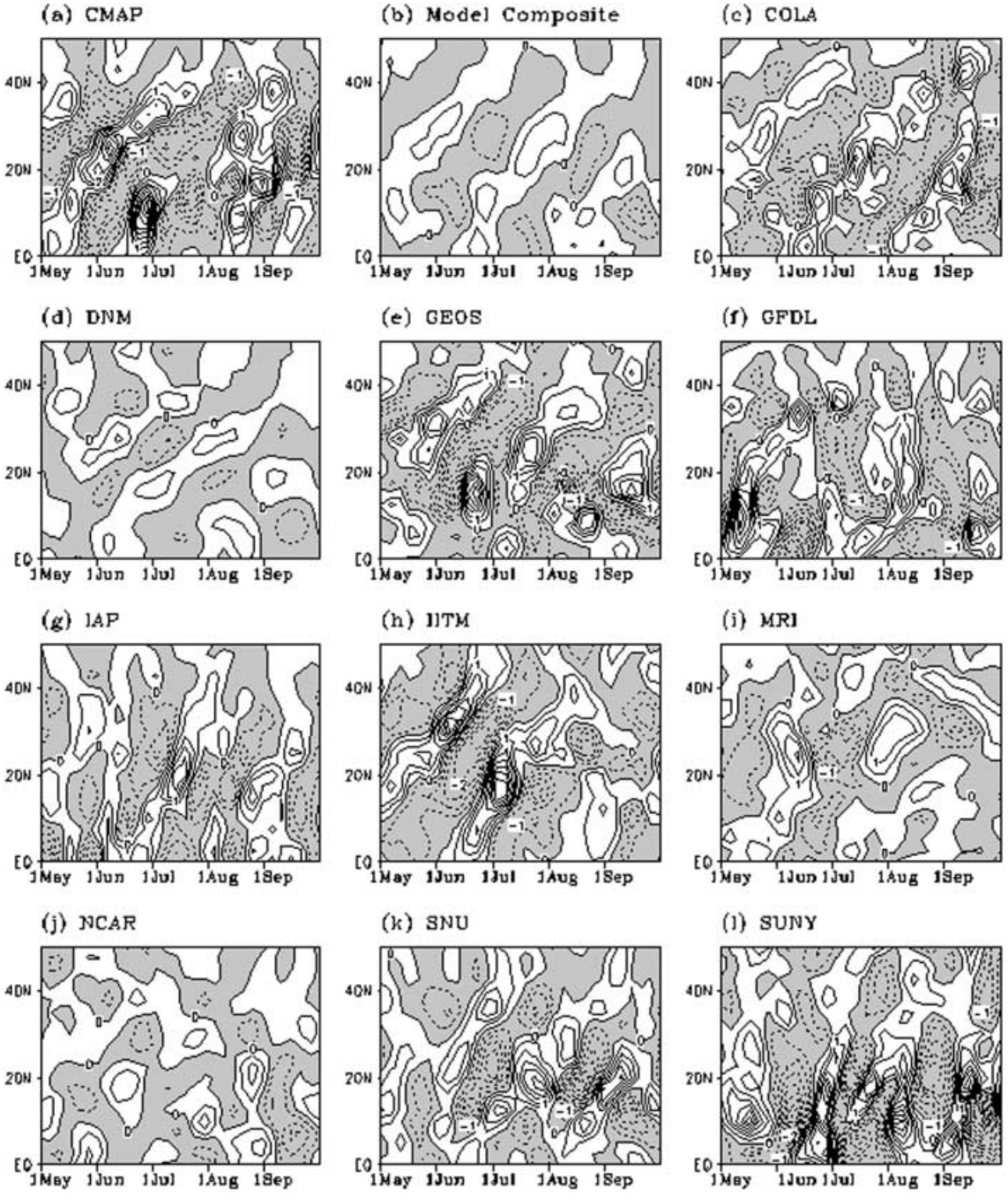

Fig. 10. Time-latitude cross sections of the climatological intraseasonal component of precipitation along 130°E: **a** and **b** are for the CMAP and the model composite, respectively, and **c**–**l** for each model. Contour interval is 0.5 mm day^{-1} and negative values are *shaded*

monsoon rainfall. The aforementioned results are consistent with Gadgil and Sajani (1998), who found that realistic simulations of monsoon variability in AMIP models are strongly dependent on their abilities to reproduce the meridional migration of the monsoon rain in the western Pacific region.

None of the models reproduces the observed rain band in the region from the East China Sea to the mid Pacific, i.e., the Mei-yu rain band. Most models simulate the rain band shifted toward the continental side along East Asia and a dry zone extending from the Sea of Okhotsk to the Korean peninsula. This situation is similar to results from a previous AMIP-I intercomparison (Lau et al. 1996), suggesting the importance of the midlatitude stationary wave pattern associated with the fluctuation of the East Asia jet stream. The influence of the East Asian jet stream on East Asian monsoon variability also has been confirmed by Liang et al. (2001). The poor simulation of the Mei-yu rain band indicates that that model simulations of the East Asian

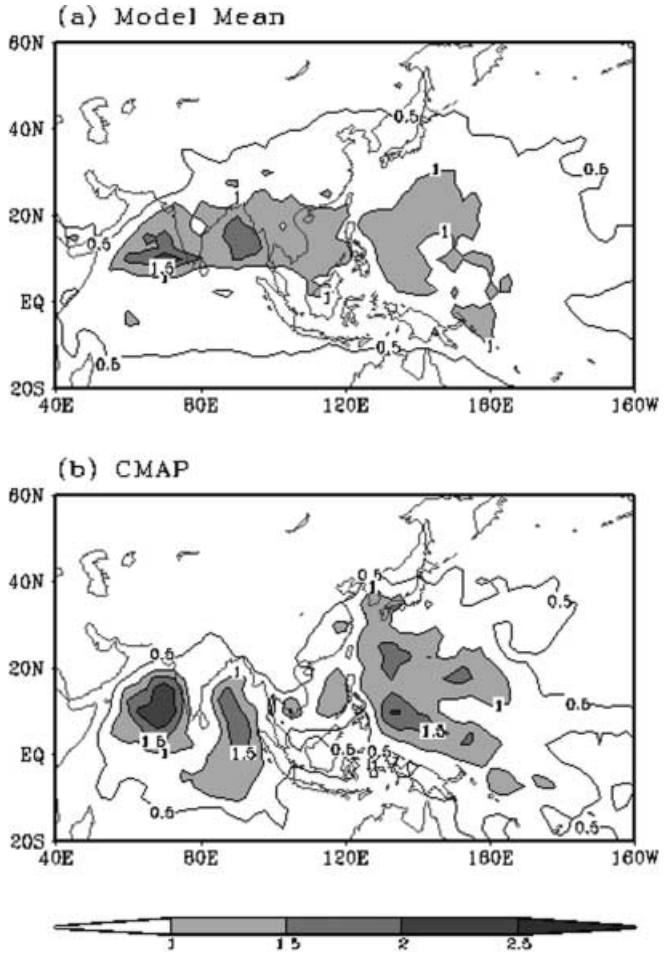

Fig. 11a, b. Standard deviations of the climatological intraseasonal oscillation (CISO) of precipitation for the five summer months. The CISO is obtained by removing the smoothed seasonal variation (sum of the first four harmonics) from the original climatological variation. Contour interval is 0.5 mm day^{-1}

monsoonthe model representation of physical processes leading to the summertime East Asian jet stream variability has not been improved since AMIP-I.

The amplitudes of climatological variations from May to September follow the intensity of climatological summer means. Accordingly, most models overestimate the amplitude of the climatological variability in the Indian region. In the western Pacific, on the other hand, most of the models underestimate the climatological variation. In particular, the model variations of DNM, NCAR, MRI, and GEOS are significantly weaker than the observed. Using the criteria based on the amplitude of the climatological variation of rainfall (Wang and Lin 2002), we have examined the domain of monsoon region produced by individual models (not shown). As in the observations, all of the models include the Indian region as part of the monsoon domain. On the other hand, several models fail to include the subtropical western Pacific in the monsoon domain.

The climatological intraseasonal variations of precipitation are also examined over the Indian region and the East Asia-western Pacific monsoon region. The spatial distribution of the averaged amplitude of the *tropical* CISO component simulated by the models is similar to the observed. However, the present models simulate the *extratropical* CISO, that are much weaker than the observed. In the Indian monsoon region, the relatively large amplitudes of the observed CISO are well simulated by the models. However, over the tropical Indian ocean region, particularly in the Southern Hemisphere, the simulated CISOs are much weaker than the observed. It is noted that, in the observations, the northward propagations of wet and dry events are evident in the extratropics between 15°N and 40°N during the summer. The northward movement of the extratropical rain band strongly affects the East Asian rainy season in East Asia, particularly eastern China, Korea, and Japan (Kang et al. 1999). This extratropical character is largely missing in the model composite. Although several models such as COLA, GEOS, IITM, and SNU show the northward moving CISO components, their phases are shifted by 20–30 days such that the models simulate an early onset of the East Asian monsoon.

An important documentation of the present intercomparison is that the climatological mean and variability of all models are exaggerated in the Indian region, whereas they are weak over the subtropical western Pacific region in most of the models. The weak simulations of the western Pacific variability may be due to the use of atmospheric GCM with prescribed SSTs. The climatological variations in the western Pacific are controlled mainly by an ocean–atmosphere coupled system and the coupled mode cannot be simulated in an atmospheric GCM alone. Thus, a coupled ocean–atmosphere model intercomparison with a focus on the monsoon simulation is a natural extension of the present study. On the other hand, the Indian monsoon rainfall may be controlled largely by land process, and both the climatological mean and variations may be exaggerated by deficiencies in the parametrized land processes in the models.

Acknowledgements The authors appreciate the participating GCM groups of CLIVAR/Monsoon GCM intercomparison project. The first and second authors have been supported by Climate Environment System Research Center (CES) sponsored by the Korean Science and Engineering Foundation and the Brain Korea 21 Program.

References

Arakawa A, Schubert WH (1974) Interaction of a cumulus cloud ensemble with the large-scale environment, part I. J Atmos Sci 31: 674–701

Betts AK (1986) A new convective adjustment scheme. Part I: observational and theoretical basis. Q J R Meteorol Soc 112: 677–691

Boyle JS (1998) Intercomparison of interannual variability of the global 200-hPa circulation for AMIP simulations. J Clim 11: 2505–2529

Gadgil S, Sajani S (1998) Monsoon precipitation in the AMIP runs. Clim Dyn 14: 659–689

Gates WL, Boyle JS, Covey C, Dease CG, Doutriaux CM, Drach RS, Fiorino M, Gleckler PJ, Hnilo JJ, Marlais SM, Phillips TJ, Potter GL, Santer BD, Sperber KR, Taylor KE, Williams DN

(1999) An overview of the results of the atmospheric model intercomparison project (AMIP1). Bull Am Meteorol Soc 80: 29–55

Goswami (1998) Interannual variations of Indian summer monsoon in a GCM: external conditions versus internal feedbacks. J Clim 11: 501–522

Gregory D, Rowntree PR (1990) A mass flux convection scheme with representation of cloud ensemble characteristics and stability dependent closure. Mon Weather Rev 118: 1483–1506

Gruber A, Su X, Kanamitsu M, Schemm J (2000) The comparison of two merged rain gauge–satellite precipitation datasets. Bull Am Meteorol Soc 81: 2631–2644

Ho CH, Kang IS (1988) The variability of precipitation in Korea. J Korean Meteorol Soc 24: 38–48

Ju JH, Slingo J (1995) The Asian summer monsoon and ENSO. Q J R Meteorol Soc 121: 1133–1169

Kalnay E, Kanamitsu M, Kistler R, Collins W, Deaven D, Gandin L, Iredell M, Saha S, White G, Woollen J, Zhu Y, Leetmaa A, Reynolds B, Chelliah M, Ebisuzaki W, Higgins W, Janowiak J, Mo KC, Ropelewski C, Wang J, Jenne R, Joseph D (1996) The NCEP/NCAR 40-year reanalysis project. Bull Am Meteorol Soc 77: 437–471

Kang IS, An SI, Joung CH, Yoon SC, Lee SM (1989) 30–60 day oscillation appearing in climatological variation of outgoing longwave radiation around East Asia duting summer. J Korean Meteorol Soc 25: 149–160

Kang IS, Ho CH, Lim YK, Lau KM (1999) Principal modes of climatological seasonal and intraseasonal variations of the Asian summer monsoon. Mon Weather Rev 127: 322–339

Kang IS, Jin K, Lau KM, Shukla J, Krishnamurthy V, Schubert SD, Wailser DE, Stern WF, Satyan V, Kitoh A, Meeh GA, Kanamitsu M, Galin VY, Kim JK, Sumi A, Wu G, Liu Y (2002) Intercomparion of atomospheric GCM simulated anomalies associated with the 1997–98 El Niño. J Clim (in press)

Krishnamurti TN (1985) Summer monsoon experiment-a review. Mon Weather Rev 113: 1590–1626

Lal M, Cubasch U, Perlwitz J, Waszkewitz J (1997) Simulation of the Indian monsoon climatology in the ECHAM3 climate model : sensitivity to horizontal resolution. Int J Climatol 17: 847–858

Lau KM, Li TM (1984) The monsoon of East Asia and its global association – a survey. Bull Am Meteorol Soc 65: 114–125

Lau KM, Yang S (1996) The Asian monsoon and predictability of the tropical ocean–atmosphere system. Q J R Meteorol Soc 122: 945–957

Lau KM, Yang GJ, Shen S (1988) Seasonal and intraseasonal climatology of summer monsoon rainfall over East Asia. Mon Weather Rev 116: 18–37

Lau KM, Kim JH, Sud Y (1996) Intercomparison of hydrologic processes in AMIP GCMs. Bull Am Meteorol Soc 77: 2209–2227

Liang XZ, Samel AN, Wang WC (1995) Observed and GCM simulated decadal variability of monsoon rainfall in east China. Clim Dyn 11: 103–114

Liang XZ, Wang WC, Samel AN (2001) Biases in AMIP model simulations of the east China monsoon system. Clim Dyn 17: 291–304

Manabe S, Smagorinsky J, Strickler RF (1965) Simulated climatology of a general circulation model with a hydrologic cycle. Mon Weather Rev 93: 769–798

Martin M (1999) The resolution of the Asian summer monsoon, and its sensitivity to horizontal resolution, in the UK meteorological office unified model. Q J R Meteorol Soc 125: 1499–1525

Moorthi S, Suarez MJ (1992) Relaxed Arakawa-Schubert: a parametrization of moist convection for general circulation models. Mon Weather Rev 120: 978–1002

Nakazawa T (1992) Seasonal phase lock of intraseasonal variation during the Asian summer monsoon. J Meteorol Soc Japan 70: 257–273

Parker DE, Jackson M, Horton EB (1995) The GISST 2.2 sea surface temperature and sea-ice climatology. CERT No. 63, Hadley Centre for Climate Prediction and Research, Bracknell, UK

Ramesh KJ, Rao PLS, Mohanty UC (2000) A Study on the performance of the NCMRWF analysis and forecasting system during Asian summer monsoon: thermodynamic aspects. Clim Dyn 154: 141–162

Reynolds RW, Smith TM (1994) Improved global sea surface temperature analyses using optimum interpolation. J Clim 7: 929–948

Slingo JM, Sperber KR, Boyle JS, Ceron JP, Dix M, Dugas B, Ebisuzaki W, Fyfe J, Gregory D, Gueremy JF, Hack J, Harzallah A, Inness P, Kitoh A, Lau WKM, McAvaney B, Madden R, Matthews A, Palmer TN, Park CK, Randall D, Renno N (1996) Intraseasonal oscillations in 15 atmospheric general circulation models: results from an AMIP diagnostic subproject. Clim Dyn 12: 325–357

Soman MK, Slingo J (1997) Sensitivity of the Asian summer monsoon to aspects of sea surface temperature anomalies in the tropical Pacific Ocean. Q J R Meteorol Soc 123: 309–336

Sperber KR, Palmer TN (1996) Interannual tropical rainfall variability in general circulation model simulations associated with the Atmosphere Model Intercomparison Project. J Clim 9: 2727–2750

Sperber KR, Hameed S, Potter GL, Boyle JS (1994) Simulation of the northern summer monsoon in the ECMWF model: sensitivity to horizontal resolution. Mon Weather Rev 122: 2461–2481

Sperber KR, Slingo JM, Annamalai H (2000) Predictability and the relationship between subseasonal and interannual variability during the Asian summer monsoon. Q J R Meteorol Soc 126: 2545–2574

Shukla JM, Fennessy J (1994) Simulation and predictability of monsoons. Proc the Int. Conf Monsoon Variability and Prediction. Tech Rep WCRP-84, WCRP, Geneva, Switzerland, pp 567–575

Tanaka M (1992) Intraseasonal oscillation and the onset and retreat dates of the summer monsoon over East, Southwest and the western North Pacific region using GMS high cloud amount data. J Meteorol Soc Japan 70: 613–629

Tao S, Chen L (1987) A review of recent research on the East Asian summer monsoon in China. In: Chang CP, Krishnamurti TN (eds) Monsoon meteorology. Oxford University Press, Oxford, UK, pp 60–92

Tao SY, Ding YH (1981) Observational evidence of the influence of the Qinhai-Xizang (Tibet) plateau on the occurrence of heavy rain and severe storms in China. Bull Am Meteorol Soc 62: 23–30

Wang B, Xu X (1997) Northern Hemisphere summer monsoon singularities and climatological intraseasonal oscillation. J Clim 10: 1071–1085

Wang B, Lin H (2002) Rainy seasons of the Asian-Pacific monsoon defined using a single variable. J Clim 15: 386–398

Wang B, Wu R, Lau KM (2001) Interannual variability of Asian summer monsoon: contrast between the Indian and western North Pacific summer monsoon. J Clim 14: 4073–4090

Webster PJ, Magana VO, Palmer TN, Shukla J, Tomas RA, Yanai M, Yasunari T (1998) Monsoons: processes, predictability, and the prospects for prediction. J Geophys Res 103: 14,451–14,510

Xie P, Arkin PA (1997) Global precipitation: a 17-year monthly analysis based on gauge observation, satellite estimates and numerical model outputs. Bull Am Meteorol Soc 78: 2539–2558

Zachary AE, Randall DA (1999) Sensitivity of the simulated Asian summer monsoon to parametrized physical processes. J Geophys Res 104: 12,177–12,191

Zhang GJ, McFarlane NA (1995) Sensitivity of climate simulations to the parametrization of cumulus convection in the Canadian Climate Centre general circulation model. Atmos–Ocean 33: 407–446

Zhang Y, Sperber KR, Boyle JS, Dix M, Ferranti L, Kitoh A, Lau KM, Miyakoda K, Randall D, Takacs L, Wetherald R (1997) East Asian winter monsoon: results from eight AMIP models. Clim Dyn 13: 792–820